Research Article

Simulation of unsteady flow in viscoelastic pipes

M. Firkowski[1] · K. Urbanowicz[1] · H. F. Duan[2]

Abstract
The paper focuses on modeling of unsteady flows in a hydraulic system built of a pressure tank, a plastic pipeline and a quick-closing valve. The influence of unsteady friction as well as the experimentally obtained creep function (necessary for modeling retarded strains) on simulation results was investigated. In addition, the effectiveness of the dimensionless parameter *P* known from the literature was analyzed, especially in the context of rejecting an unsteady term decision. Detailed investigations on the variability of terms describing unsteady friction have shown that one should still look for a dimensionless parameter with the help of which it will be possible to decide on the friction model before making the calculations. The quantitative analysis carried out showed that the use of unsteady hydraulic resistance in simulated runs brought simulated results closer to experimental results.

Keywords Water hammer · Viscoelastic pipe · Unsteady flow · Method of characteristics · Frequency dependent friction

1 Introduction

Plastics are starting to play an increasingly important role in hydraulic systems each year. As of today, most of the hydraulic elements can be made of them [24]. Plastic pipes almost completely replaced metal pipes (steel, brass, etc.) in water supply systems. This was mainly due to their low price. They are produced from at least five different polymers: PP—polypropylene, PE—polyethylene, PVC—polyvinyl chloride, PB—polybutylene, ABS—acrylonitrile butadiene styrene. Each of the above-mentioned materials is characterized by different mechanical properties (Poisson's ratio, Young's modulus of elasticity, creep function, etc.), whose values strongly depend on the temperature. In these pipelines, as well as in metal, transient states may occur during the flow of liquids. From previous work carried out by the authors of this study [28–31], it turned out that the phenomena accompanying unsteady flows in metal pipelines such as: cavitation [1, 7, 14, 21, 35], unsteady friction [5, 13, 25–27] or the interaction of the walls of the pipe with the flow (fluid structure interaction) [9, 11, 16] also plays an important role in plastic pipes. The phenomenon that is most responsible for flow damping is the viscoelasticity of the material of the pipe [2, 10, 28–31]. Attempts to simulate the flow using a model for elastic pipes result in an unacceptable discrepancy between simulation and experimental results. Thermal phenomena [17, 18] are usually neglected during the modeling of the examined transient flow (water hammer) in this paper (e.g., result of sudden blockage of flow). As proved in [2, 10], the application of the calibration enables satisfactory model compliance to be obtained using the quasi-steady model of hydraulic resistance. The need to calibrate the creep function is mainly due to the lack of accurate experimental studies on their course in time (frequency) and temperature. In this paper, a modified unsteady flow model will be used, which properly takes into account frequency dependent hydraulic resistance. Unsteady flows in two experimental systems in HDPE pipelines were analyzed. Viscoelastic damping was modeled using the experimental creep function known from the literature [4]. According to paper [8], one can specify a

✉ M. Firkowski, mateusz.firkowski@zut.edu.pl; K. Urbanowicz, kamil.urbanowicz@zut.edu.pl; H. F. Duan, hf.duan@polyu.edu.hk | [1]Department of Mechanical Engineering and Mechatronics, West Pomeranian University of Technology Szczecin, Piastów 19, 70-310 Szczecin, Poland. [2]Department of Civil and Environmental Engineering, The Hong Kong Polytechnic University, Hung Hom, Kowloon 999077, Hong Kong.

SN Applied Sciences (2019) 1:519 | https://doi.org/10.1007/s42452-019-0524-2

Received: 5 February 2019 / Accepted: 25 April 2019 / Published online: 6 May 2019

certain dimensionless parameter P, which is dependent on internal diameter, pressure wave speed, friction factor, velocity and length of the pipe. Some authors [6, 15, 33] use this parameter to determine the use of friction model. In this work, a transient flow model will be used, dedicated to plastic pipes, discussed in detail in [28, 30]. Analysis of the results obtained will demonstrate the need of using unsteady hydraulic resistance.

2 Water hammer in viscoelastic pipes

This section is devoted to introduce the equations describing water hammer in viscoelastic pipes and presentation of numerical solutions.

2.1 Mathematical model

Polymer pipelines do not respond according to Hook law when subjected to a certain instantaneous stress. Strain can be decomposed into a sum of instantaneous elastic strain ε_e and a retarded strain ε_r (see e.g., [3])

$$\varepsilon(t) = \varepsilon_e + \varepsilon_r(t). \tag{1}$$

The retarded strain is a convolution integral of pressure and derivative of the creep function J which describes viscoelastic behavior of the pipe material

$$\varepsilon_r(t) = \frac{\Xi}{2}\int_0^t (p(t-u)-p(0))\frac{\partial J(u)}{\partial u}\mathrm{d}u, \tag{2}$$

where $\Xi = \frac{\alpha D}{e}$—enhanced pipe wall constraint coefficient parameter [−], D—pipe inside diameter [m], e – pipe wall thickness [m], α—pipe wall constraint coefficient [–], $J(u)$—polymer creep function $\left[\mathrm{Pa}^{-1}\right]$.

The creep function in generalized Kelvin–Voigt (Fig. 1) model is time dependent, namely

$$J(t) = J_0 + \sum_{i=1}^{k} J_i\left(1 - e^{-\frac{t}{T_i}}\right), \tag{3}$$

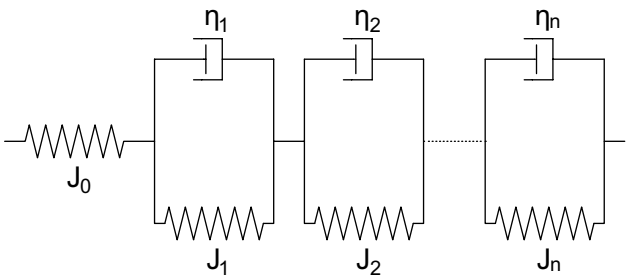

Fig. 1 Generalized Kelvin Voigt model (viscoelastic solid)

where J_i—creep compliance of the spring of the Kelvin–Voigt i-th element defined by $J_k = 1/E_k$, E_k—modulus of elasticity of the spring of i-th element, T_i—the retardation time of the dashpot of i-th element.

Equation (2) can be written in the form [30]

$$\varepsilon_r(t) = \frac{\Xi}{2}\int_0^t (p(t-u)-p(0))\cdot w_J(u)\mathrm{d}u \tag{4}$$

and its partial derivative with respect to time t as

$$\frac{\partial \varepsilon_r(t)}{\partial t} = \frac{\Xi}{2}\int_0^t \frac{\partial}{\partial t}(p(t-u)-p(0))\cdot w_J(u)\mathrm{d}u, \tag{5}$$

where $w_J(u)$ denotes creep weighting function and

$$w_J(u) = \sum_{i=1}^{k}\frac{J_i}{T_i}e^{-\frac{u}{T_i}}. \tag{6}$$

In unsteady flow in pipe, the instantaneous wall shear stress τ may be regarded as the sum of two components [32]:

$$\tau = \underbrace{\frac{\rho v|v|}{8}\lambda}_{\tau_q} + \underbrace{\frac{2\mu}{R}\int_0^t w(t-u)\frac{\partial v}{\partial t}(u)\mathrm{d}u}_{\tau_u}, \tag{7}$$

where λ—Darcy–Weisbach friction factor [−], $w(t)$ – weighting function [−], μ—dynamic viscosity $\left[\frac{\mathrm{kg}}{\mathrm{m\,s}}\right]$, u—time, used in convolution integral [s].

The first component in (7), τ_q, presents the quasi–steady wall shear stress and the second, τ_u, is the additional contribution due to unsteadiness. Equation (7) relates the wall shear stress to the instantaneous average velocity and to the weighted past velocity changes.

Unsteady flow of liquid in viscoelastic pipe is represented by two one-dimensional hyperbolic partial differential equations. The momentum and continuity equations have the following form [31]

$$\begin{aligned} \rho\tfrac{\partial v}{\partial t} + \tfrac{\partial p}{\partial x} + \tfrac{2}{R}\tau &= 0,\\ \tfrac{1}{\rho c^2}\tfrac{\partial p}{\partial t} + \tfrac{\partial v}{\partial x} + 2\tfrac{\partial \varepsilon_r}{\partial t} &= 0, \end{aligned} \tag{8}$$

where t—time [s], x—distance along the pipe axis [m], $v = v(x,t)$—average value of velocity in cross-section of pipe [m/s], $p = p(x,t)$—average value of pressure in cross-section of pipe [Pa], τ—shear stress at pipe wall [Pa], ρ—density of liquid (constant) [kg/m^3], R—inside radius of pipe [m], c—pressure wave speed [m/s].

2.2 Numerical solution

There is no known analytical solution for system of hyperbolic partial differential equations (8). Therefore, there is a need to perform calculations using numerical methods. In this paper, a method of characteristics and finite difference method with classic constant rectangular grids is used, to avoid interpolation problems (Fig. 2).

At the beginning, the initial conditions of the system will be discussed. In a pre-transient state, the mean velocity v_0 is constant on whole length of pipe $x = L$. The reservoir pressure (at $x = 0$) is constant and decreases linearly in the direction of the flow. At $t = 0$, the valve closes suddenly ($x = L$) causing transient states, and the velocity changes from v_0 to 0 in one time step. After that, the pressure oscillation of fluid occurs until the full suppression. The final conditions on the entire pipe are $v = 0$ and $p = p_A$ (constant reservoir pressure).

Now one can proceed to the numerical solution. The system of differential equations (8) was solved using method of characteristics. Thanks to this, the system of partial differential equations was transformed into two ordinary differential equations

$$\pm\frac{1}{\rho c}\frac{\mathrm{d}p}{\mathrm{d}t}+\frac{\mathrm{d}v}{\mathrm{d}t}+\frac{2}{\rho R}\tau+2c\frac{\partial\varepsilon}{\partial t}=0 \quad \text{if} \quad \frac{\mathrm{d}x}{\mathrm{d}t}=\pm c. \tag{9}$$

Using the finite difference method on characteristics grid (Fig. 2), it was obtained

$$\begin{aligned}\tfrac{1}{c\rho}(p_D-p_L)+(v_D-v_L)+\tfrac{2\Delta t}{\rho R}\tau_L+2c\Delta t\tfrac{\partial\varepsilon_D}{\partial t} &= 0,\\ -\tfrac{1}{c\rho}(p_D-p_R)+(v_D-v_R)+\tfrac{2\Delta t}{\rho R}\tau_R-2c\Delta t\tfrac{\partial\varepsilon_D}{\partial t} &= 0,\end{aligned} \tag{10}$$

where Δt—constant time step [s]. The term connected with strain rate is calculated as follows [30]

$$\frac{\partial\varepsilon_D}{\partial t}=\frac{\Xi}{2}\sum_{k=1}^{n}\underbrace{\left(x_E B_k+A_k p_D-A_k p_E\right)}_{x_D}=p_D F-G_E, \tag{11}$$

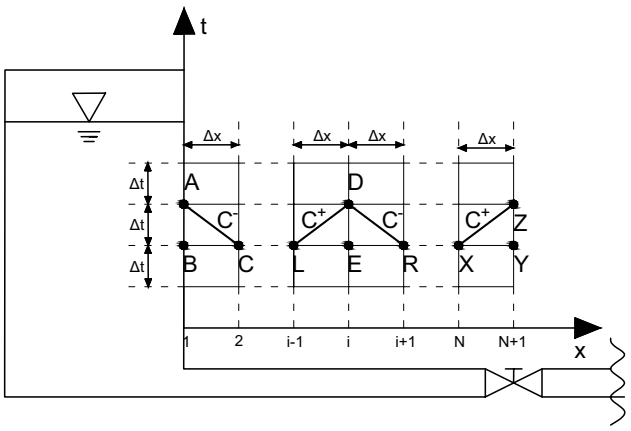

Fig. 2 Rectangular grid of characteristics

with constants

$$\begin{aligned}A_k &= \frac{J_i}{\Delta t}\left(1-e^{-\frac{\Delta t}{T_i}}\right), B_k = e^{-\frac{\Delta t}{T_i}},\\ F &= \frac{\Xi}{2}\sum_{k=1}^{n}A_k, G_E = \frac{\Xi}{2}\sum_{k=1}^{n}\left(A_k\cdot p_E - x_E\cdot B_k\right).\end{aligned}$$

Let now denote all the terms calculated for the previous time step as

$$\begin{aligned}C_L &= v_R+\tfrac{p_L}{\rho c}-\tfrac{2\Delta t}{\rho R}\tau_L+2c\Delta t G_E,\\ C_R &= v_R-\tfrac{p_R}{\rho c}-\tfrac{2\Delta t}{\rho R}\tau_R-2c\Delta t G_E.\end{aligned} \tag{12}$$

Finally, one gets a numerical solution for pressure and flow velocity

$$p_D=\frac{C_L-C_R}{\left(\frac{2}{\rho c}+4cF\Delta t\right)} \quad \textit{and} \quad v_D=\frac{C_L+C_R}{2}. \tag{13}$$

The formulas for pressure and velocity at the pipe ends will now be derived. For the reservoir ($x = 0$), the negative characteristics C^- are used (Fig. 2). Let us assume that the pressure is constant ($p = p_A$) and therefore, one needs the formula for velocity only. Using the second equation from (10), one obtains for the left boundary

$$v_A=\frac{1}{c\rho}\left(p_A-p_C\right)+v_C-\frac{2\Delta t}{\rho R}\tau_C. \tag{14}$$

For the valve ($x = L$), the positive characteristics C^+ are used. Let us assume that the velocity is constant ($v_Z = 0$) so one needs the formula for pressure. Using the first equation from (10), one obtains

$$p_Z=p_X+c\rho v_X+\frac{2c\Delta t}{R}\tau_X+2c^2\Delta t\rho\frac{\partial\varepsilon_Z}{\partial t}. \tag{15}$$

Numerical calculations of time dependent of the wall shear stress τ_u [second component in (7)] can be performed using the efficient numerical solution of this integral presented by Urbanowicz [27]

$$\begin{aligned}&\tau_u(t+\Delta t)\\ &=\frac{2\mu}{R}\sum_{i=1}^{j}\underbrace{\left[y_{i(t)}A_i+\eta B_i\left[v_{(t+\Delta t)}-v_{(t)}\right]+[1-\theta]C_1\left[v_{(t)}-v_{(t-\Delta t)}\right]\right]}_{y_{i(t+\Delta t)}},\end{aligned} \tag{16}$$

where

$$A_i=\mathrm{e}^{-n_i\Delta\hat{t}},\ B_i=\tfrac{m_i}{n_i\Delta\hat{t}}\left[1-A_i\right],\ C_i=A_iB_i.$$

The constants n_i and m_i present in the above equations are associated with the effective weighting function

$$w(\hat{t}) = \sum_{i=1}^{k} m_i e^{-n_i \hat{t}} \tag{17}$$

and θ is the correction factor [25].

3 Simulations

3.1 Experimental setup

To verify carried out numerical simulations, they were compared with experimental data. The experiments were carried out by D. Covas et al. at Imperial College London [3] and Evangelista et al. at the University of Cassino and Southern Lazio [6].

The first experimental reservoir-pipeline-valve system [3] consists of a 271.7 m HDPE pipe with an internal diameter 50.6 mm and 6.3 mm wall thickness. Form the analysis of observed experimental dynamical courses of pressure changes, the pressure wave speed in the tested system was determined at $c = 395$ m/s. The water temperature is $T = 20\,^{\circ}$C, on its basis, the density $\rho = 998.2\,\mathrm{kg/m^3}$ and kinematic viscosity $\nu = 1 \times 10^{-6}\,\mathrm{m^2/s}$ were determined. The Poisson's ratio of the material from which the pipeline is made was $\nu_P = 0.46$. Other input parameters for numerical calculations are summarized in Table 1. Parameters T_k and J_k of the Kelvin–Voigt models experimentally determined by Covas [4] have values presented in Table 2 (see Case 1, 3). The pipe wall constraint coefficient is calculated form the following formula [3]

$$\alpha = \frac{2e}{D}\left(1 + \nu_P\right) + \frac{D}{D+e}\left(1 - \nu_P^2\right) \tag{18}$$

and for this test stand have a fixed value $\alpha = 1.0647$.

The second test stand was built to investigate the transient states in branched systems of HDPE pipes [6]. The system was inspired by irrigation system and is Y-shaped with three-way junction. The authors carried out preliminary experiments in single-pipe systems, which were used in this paper. The experimental system consists of a 203.3 m HDPE pipe with internal diameter 44 mm and wall thickness 3 mm. The average value of propagation of the pressure wave speed was determined at 368 m/s. The water temperature is $T = 14.95\,^{\circ}$C, on its basis, the density $\rho = 999.1\,\mathrm{kg/m^3}$ and kinematic viscosity $\nu = 1.14 \times 10^{-6}$ $\mathrm{m^2/s}$ were determined. The authors of the original reference did not mention the value of Poisson's ratio, so it was assumed the same value as Covas for HDPE pipes, i.e., $\nu_P = 0.46$. The pipe wall constraint coefficient $\alpha = 0.9372$ was calculated using equation (18). To describe the creep function, the results of the Covas experiment were used. Parameters T_k have been set as above. However, the J_k parameters have been scaled based on the results of the Güney experiment [30]. Güney determined the parameters of the creep function at different temperatures. The scaling factor was assumed to be 0.75 which gave values presented in Table 2 (see Case 2, 4).

Table 2 Creep compliance coefficients J_k

Parameter	$k = 1$	$k = 2$	$k = 3$	$k = 4$	$k = 5$
Case 1, 3					
$J_k\left(10^{-9}Pa^{-1}\right)$	0.1394	0.0062	0.1148	0.3425	0.0928
$T_k\,(s)$	0.05	0.5	1.5	5	10
Case 2, 4					
$J_k\left(10^{-9}Pa^{-1}\right)$	0.1046	0.0046	0.0861	0.2569	0.0696
$T_k\,(s)$	0.05	0.5	1.5	5	10

3.2 Comparison of experimental results and numerical simulations

To evaluate the effect of unsteady friction on the modeled pressure waves, numerical simulations were carried out for four different cases. Two of them concerned laminar flow and the other two were turbulent. In addition, the dimensionless parameter P defined by Ghidaoui et. al [8]

$$P = \frac{2Dc}{\sqrt{\lambda} v_0 L}, \tag{19}$$

were examined. The values of this parameter for the analyzed below the selected flows are shown in Table 1.

As described in paper [8], the physical meaning of the parameter P is the ratio of the diffusion time scale to the wave time scale in water hammer problems. When $P \gg 1$,

Table 1 Parameters of experimental tests

Case	L [m]	D [mm]	e [mm]	ν_P	c [m/s]	v_0 [m/s]	Re_0 [−]	P_0 [−]
1	271.1	50.6	6.3	0.46	395	0.0268	1356	25.27
2	203.3	44.0	3.0	0.46	368	0.0635	2451	15.52
3	271.1	50.6	6.3	0.46	395	0.7459	37743	1.31
4	203.3	44.0	3.0	0.46	368	1.0000	38596	1.06

the quasi-steady friction model is acceptable. When $P \approx 1$, it has been indicated that a unsteady friction model should be used. When $P \ll 1$, it does not belong to the water hammer problems, so similarly the quasi-steady friction model should be acceptable.

In Case 1 and 3, the pipeline was divided into 64 equally long sections ($N = 64\,[-]$, $\Delta x = 4.2453$ [m]). According to the CFL condition, the constant time step is $\Delta t = 0.0107$ s ($\Delta \hat{t} = 1.6791 \times 10^{-5}\,[-]$). For these time step values, the estimated coefficient of three term weighting function using a method described in paper [25] are $m_1 = 4.4699$, $m_2 = 15.7495$, $m_3 = 56.9421$and $n_1 = 90.0521$, $n_2 = 1359$, $n_3 = 18150$ for laminar flow and $n_1 = 1248$, $n_2 = 2517$, $n_3 = 19308$ for turbulent flow. In Case 2 and 4, the pipeline was divided into $N = 204$ equally long sections ($N = 204$ $[-]$, $\Delta x = 0.9966$). This division was used because the pressure transmitter with which we compare the results is about 1 meter in front of the valve. The constant time step is $\Delta t = 0.0027\,s$ ($\Delta \hat{t} = 6.3785 \cdot 10^{-6}\,[-]$) and using the procedure explained in [25] the estimated coefficient of three term weighting function are $m_1 = 7.818$, $m_2 = 25.7227$, $m_3 = 92.4308$ and $n_1 = 198.5231$, $n_2 = 3523$, $n_3 = 47696$ for laminar flow and $n_1 = 1377$, $n_2 = 4701$, $n_3 = 48875$ for turbulent flow.

Figure 3 provides detailed comparisons between measured and calculated results corresponding to the quasi-steady and unsteady friction model, which included the viscoelastic behavior of the pipe wall material. On their basis, the following conclusions can be formulated

1. The pressure peak on the first amplitude is better simulated using unsteady friction model.

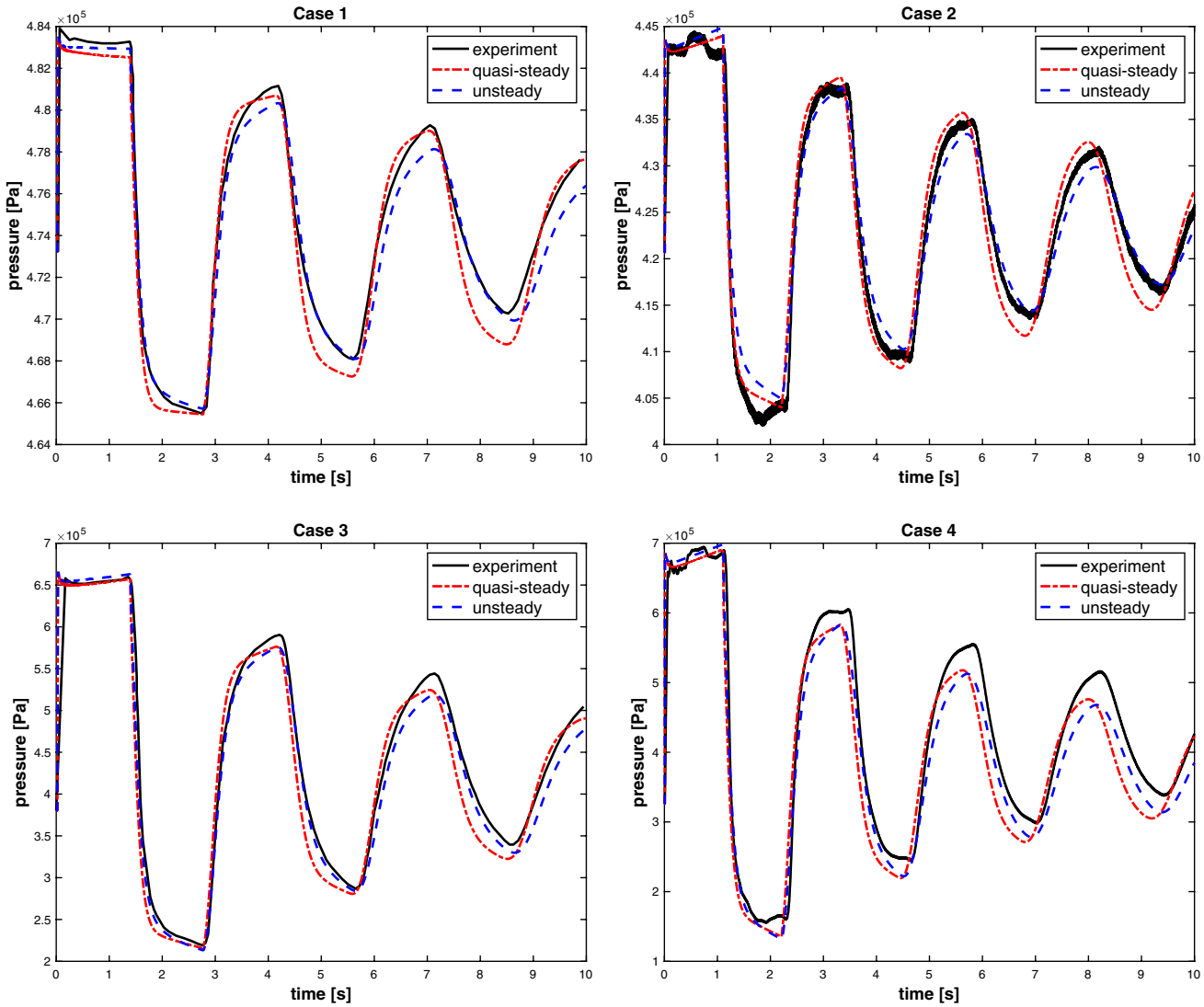

Fig. 3 Pressure variation at the downstream end of the pipe

2. On the other amplitudes, low pressures (runway valleys) are more accurately simulated with use of unsteady friction model, while high (amplitude peaks) using a quasi-steady friction model in low Reynolds number cases (Case 1 and 2).
3. Both models have a slight shifting over time. In the case of a quasi-steady friction model, the time between successive amplitudes is shortened, while in the unsteady friction model it becomes longer.
4. The qualitative analysis in laminar flow (Case 1 and 2) shows that the unsteady friction model better fits to the experimental data.
5. The qualitative analysis of turbulent flow (Case 3 and 4) shows the relative compatibility of both models.
6. The other differences observed in the comparative runs are the result of the neglecting of less significant phenomena accompanying the water hammer, as well as the result of experimental research in systems with many elbows, which are the result of increased hydraulic resistance. [23].

Figure 4 presents a comparison of dimensionless velocity ($\hat{v}(t) = v(t)/\max|v(t)|$) with a dimensionless quasi-steady wall shear stress ($\hat{\tau}_q(t) = \tau_q(t)/\max|\tau_q(t)|$) and a comparison of dimensionless acceleration ($\hat{\dot{v}}(t) = \dot{v}(t)/\max|\dot{v}(t)|$) with dimensionless unsteady wall shear stress ($\hat{\tau}_u(t) = \tau_u(t)/\max|\tau_u(t)|$) component in the middle section of the pipeline. Normalization was done in order to better present the studied phenomenon. One can observe the phase compatibility of the velocity with a quasi-steady wall shear stress component as well as phase

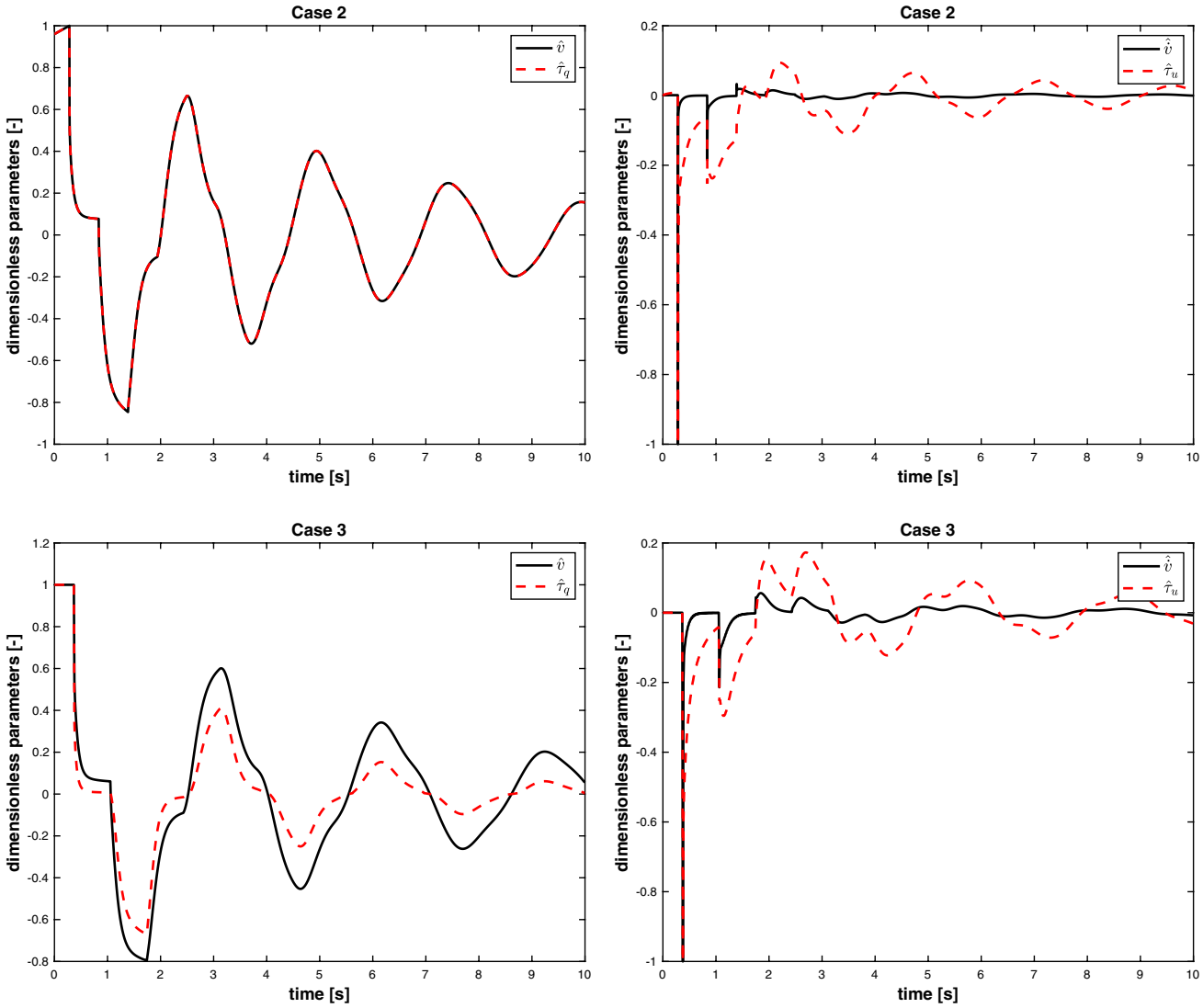

Fig. 4 Comparison of wall shear stresses for the middle of the pipe in a dimensionless form in Cases 2 (laminar) and 3 (turbulent) for unsteady friction model

compatibility of the acceleration with a unsteady wall shear stress component. Thus, the total wall shear stress is a function dependent on velocity and acceleration. The above observation is consistent with the form of wall shear stress $\tau = f(v, \dot{v})$ being the sum of two components [12, 19, 20, 22, 34]: one proportional to the average speed and the second proportional to the acceleration. In addition, one can observe coverage of dimensionless velocity and quasi-steady wall shear stress plots in laminar case. In turbulent flow, this phenomenon does not occur due to the changing nature of the flow and the use of various models of quasi-steady wall shear stress in laminar and turbulent flows. On the basis of Fig. 5, the dominant role of the unsteady wall shear stress component on total wall shear stress can be observed for low Reynolds numbers (Case 2). On the other hand, for the large values of the Reynolds number (Case 3), the role of the quasi-steady and unsteady wall shear stress component is comparable. Similar observations also take place in Cases 1 and 4. The greater the Reynolds number will be, the smaller will be the impact of the unsteady friction term τ_u.

One of the assumptions of this paper was to examine whether using the P parameter one can make decisions about the choice of the use of a hydraulic resistance model. Therefore, the dynamics of changes of this parameter in different pipe cross-sections was also investigated. Selected plots of the parameter P for the case of the unsteady friction model are shown in Fig. 6. The above plots questioned the reasonableness of using the dynamic parameter P described by the Eq. (19), because it can be seen that whenever the flow velocity dropped and a change in its value occurred (as a

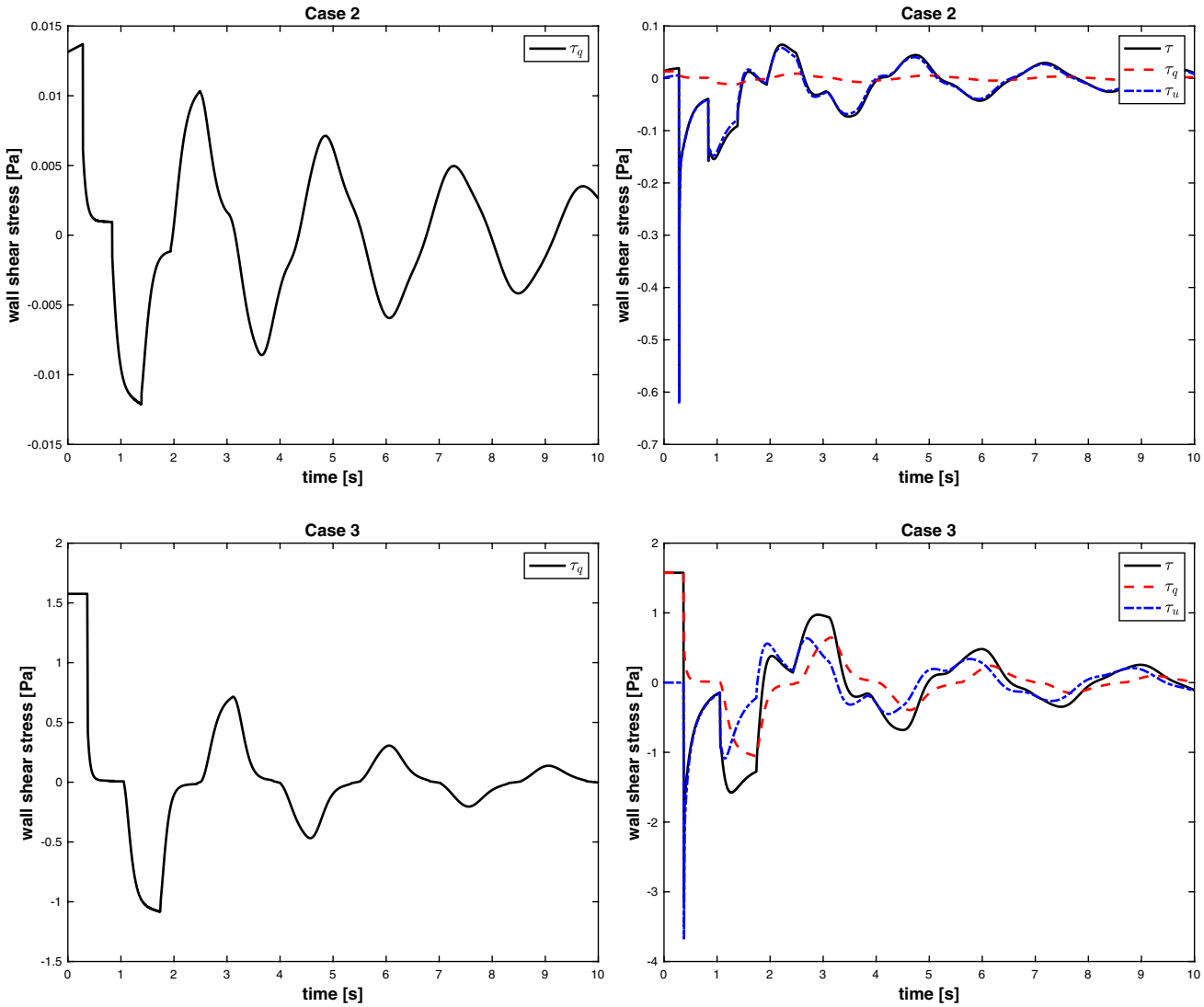

Fig. 5 Comparison of wall shear stresses in the middle of the pipe in Cases 2 and 3 for simplified quasi-steady (left) and total friction model (right) (note the different scales on the plots)

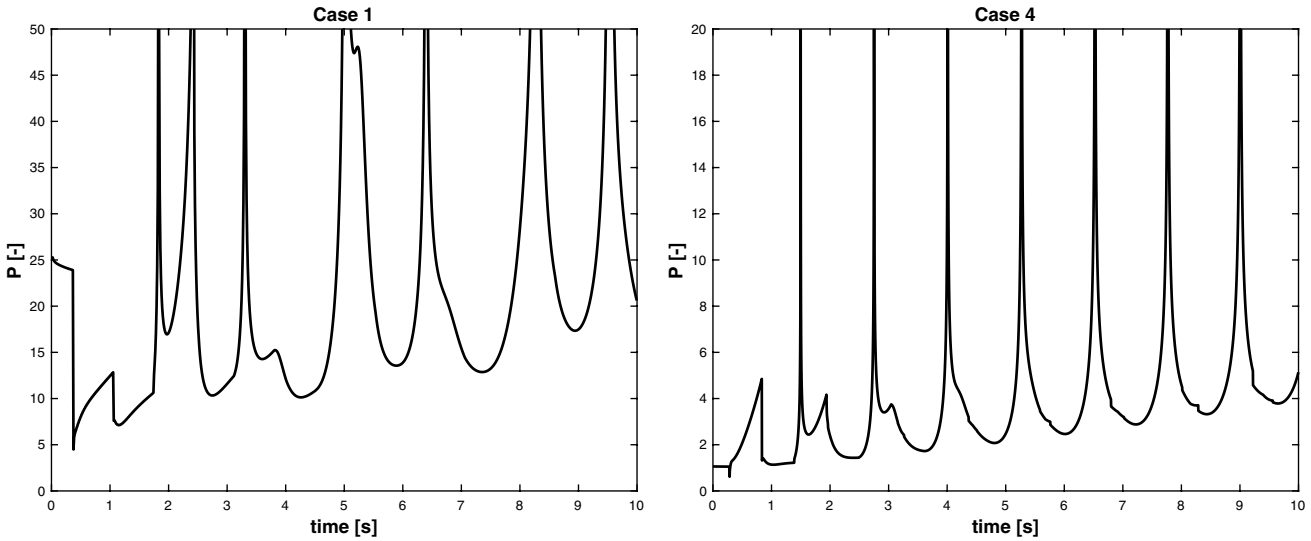

Fig. 6 Dynamic change of the parameter P in the middle of the pipe in selected cases (note the different scales on the plots)

result of a change in the flow direction), its singularities occurred. An increase in the $P > 30$ value in accordance with [6, 15, 33] should be considered a sufficient reason to reject and not designate unsteady term of friction. However, the attempt to reject the unsteady wall shear stress τ_u from Eq. (7) in a dynamic manner, carried out as part of the simulation work, was unsuccessful. Generally, it is also known that the effect of unsteady friction increases with the decreasing Reynolds number, so that the behavior of the parameter P would be contradictory to the above.

3.3 Quantitative comparative analysis

In the previous section, the results of numerical simulation was presented. Calculated values of the initial parameter P (Table 1) suggests that the better results should be obtained using the quasi-steady friction model in Cases 1 and 2, while one should obtain better results using the unsteady friction model in Cases 3 and 4, but the qualitative analysis conducted does not give a definite answer which of the friction models gives better results. To this end, L^2 norm of errors was introduced (see e.g., [2]) and denoted as $\|\cdot\|_2$. Considering numerical p_{sim} and measured experimental p_{exp} values of pressure as a vector, the L^2 norm is defined here as

$$\|p_{\text{sim}} - p_{\text{exp}}\|_2 = \sqrt{\sum_{i=1}^{N_p} \left|p_{\text{sim},i} - p_{\text{exp},i}\right|^2 \Delta t},$$

where N_p denotes the dimension of the vector p_{exp}.

Table 3 L^2 norm of errors

Case	1	2	3	4
Error				
Quasi-steady	3901	7920	84868	147923
Unsteady	3507	6508	53863	110001
Computation time				
Quasi-steady [s]	1.95	52	1.70	82
Unsteady [s]	2.30	100	2.75	125

In the all considered cases, a smaller L^2 norm of errors was obtained in numerical simulations using unsteady friction model. At the same time, the computation time is higher than in the case of a quasi-steady friction model. The details are presented in Table 3.

4 Conclusions

The paper presents further analysis of the influence of a quasi-steady and unsteady friction model in viscoelastic pipes on simulated pressure runs. The model of water hammer in viscoelastic pipes was analyzed. Additional term describing the retarded deformation of the pipe wall was added to continuity equation. System of partial differential equations describing this type of flow was numerically solved using the method of characteristics and finite difference method. The research considered a qualitative and quantitative analysis of new comparisons of experimental results [6] with simulated ones. Unfortunately, the qualitative analysis does not give definite

answers as to the validity of the hydraulic loss model used on the basis of the *P* parameter.

In the absence of a clear answer, a quantitative analysis was used. The L^2 norm of errors was introduced to compare the simulated pressure waves and results of the experiment. A detailed analysis showed that the unsteady friction model minimizes L^2 norm of errors.

The research carried out shows that further work is needed to determine proper dimensionless coefficient used for initial and following estimations of the importance of selected friction model for numerical simulations.

In addition, the paper proves that experimental creep function is suitable for numerical simulations in various systems based on HDPE polymer pipes. The flow model analyzed in this work allows simulation of transient states occurring in plastic pipes. It is especially important in the design stage of the fluid systems: hydraulic, water supply, transmission, etc., because with it the systems are optimized in the selection of physical parameters for better operation and management.

Acknowledgements The authors would like to thank Ph.D. Eng. A. Leopardi (University of Cassino and Southern Lazio), for providing the experimental data of the water hammer test problems presented in this paper.

Compliance with ethical standards

Conflict of interest The authors declare that they have no conflict of interest.

References

1. Bergant A, Karadžić U, Tijsseling A (2017) Developments in multiple-valve pipeline column separation control. J Phys Conf Ser 813:012–015
2. Bertaglia G, Ioriatti M, Valiani A, Dumbser M, Caleffi V (2018) Numerical methods for hydraulic transients in visco-elastic pipes. J Fluids Struct 81:230–254
3. Covas D, Stoianov I, Ramos H, Graham N, Maksimovic C (2004) The dynamic effect of pipe-wall viscoelasticity in hydraulic transients. Part I—experimental analysis and creep characterization. J Hydraul Res 42(5):517–531
4. Covas D, Stoianov I, Ramos H, Graham N, Maksimovic C (2005) The dynamic effect of pipe-wall viscoelasticity in hydraulic transients. Part II—model development, calibration and verification. J Hydraul Res 43(1):56–70
5. Duan HF, Meniconi S, Lee PJ, Brunone B, Ghidaoui MS (2017) Local and integral energy-based evaluation for the unsteady friction relevance in transient pipe flows. J Hydraul Eng 143(7):04017015
6. Evangelista E, Leopardi A, Pignatelli R, de Marinis G (2015) Hydraulic transients in viscoelastic branched pipelines. J Hydraul Eng 141(8):04015016
7. Gao H, Tang X, Li X, Shi X (2018) Analyses of 2d transient models for vaporous cavitating flows in reservoir-pipeline-valve systems. J Hydroinfrom 20(4):934–945
8. Ghidaoui MS, Mansour SGS, Zhao M (2002) Applicability of quasisteady and axisymmetric turbulence models in water hammer. J Hydraul Eng 128(10):917–924
9. Ghodhbano A, Haj Taïeb E (2017) A four-equation friction model for water hammer calculation in quasi-rigid pipelines. Int J Press Vessels Pip 151:54–62
10. Guidara MA, Hadj Taieb L, Schmitt C, Hadj Taieb E, Azari Z (2018) Investigation of viscoelastic effects on transient flow in a relatively long PE100 pipe. J Fluids Struct 80:370–389
11. Henclik S (2014) The boundary condition at the valve for numerical modelling of transient pipe flow with fluid structure interaction. J Phys Conf Ser 530:012–034
12. Iguchi M, Ohmi M, Akao F (1985) Time-dependent wall shear stress in a duct with arbitrary cross-section. Bull JSME 28(244):2280–2287
13. Ioriatti M, Dumbser M (2018) Semi-implicit staggered discontinuous Galerkin schemes for axially symmetric viscous compressible flows in elastic tubes. Comput Fluids 167:166–179
14. Jensen RK, Larsen JK, Lassen KL, Mandø M, Andreasen A (2018) Implementation and validation of a free open source 1d water hammer code. Fluids 3(3):64
15. Karadžić U, Bulatović V, Bergant A (2014) Valve-induced water hammer and column separation in a pipeline apparatus. Stroj Vestn J Mech E 60(11):742–754
16. Li S, Karney BW, Liu G (2015) FSI research in pipeline systems—a review of the literature. J Fluids Struct 57:277–297
17. Muszynski T, Andrzejczyk R (2016) Heat transfer characteristics of hybrid microjet–microchannel cooling module. Appl Therm Eng 93:1360–1366
18. Muszynski T, Andrzejczyk R, Dorao CA (2017) Detailed experimental investigations on frictional pressure drop of R134a during flow boiling in 5 mm diameter channel—the influence of acceleration pressure drop component. Int J Refrig 82:163–173
19. Ohmi M, Iguchi M, Usui T (1981) Flow pattern and frictional losses in pulsating pipe flow: part 5, wall shear stress and flow pattern in a laminar flow. Bull JSME 24(187):75–81
20. Ohmi M, Iguchi M, Usui T (1981) Flow pattern and frictional losses in pulsating pipe flow: part 6 frictional losses in a laminar flow. Bull JSME 24(196):1756–1763
21. Pezzinga G, Santoro VC (2017) Unitary framework for hydraulic mathematical models of transient cavitation in pipes: numerical analysis of 1d and 2d flow. J Hydraul Eng 143(12):04017053
22. Popov DN (1982) Unsteady hydromechanical processes. Mechanical Engineering, Moscow **(in Russian)**
23. Stosiak M, Zawiślak M, Nishta B (2018) Studies of resistances of natural liquid flow in helical and curved pipes. Pol Marit Res 25(3):123–130
24. Stryczek J, Banaś M, Krawczyk J, Marciniak L, Stryczek P (2017) The fluid power elements and systems made of plastics. Proc Eng 176:600–609
25. Urbanowicz K (2017) Analytical expressions for effective weighting functions used during simulations of water hammer. J Theor Appl Mech Pol 55(3):1029–1040
26. Urbanowicz K (2017) Modern modeling of water hammer. Pol Marit Res 24(3):68–77
27. Urbanowicz K (2018) Fast and accurate modelling of frictional transient pipe flow. ZAMM-Z Angew Math Mech 98(5):802–823

28. Urbanowicz K, Firkowski M (2018) Effect of creep compliance derivative in modeling water hammer in viscoelastic pipes. In: Proceedings of 13th international conference pressure surges, pp 305–324. BHR Group, Bordeaux, France (2018)
29. Urbanowicz K, Firkowski M (2018) Extended bubble cavitation model to predict water hammer in viscoelastic pipelines. J Phys Conf Ser 1101:012–046
30. Urbanowicz K, Firkowski M (2018) Modelling water hammer with quasi-steady and unsteady friction in viscoelastic pipelines. In: Awrejcewicz J (ed) Dynamical systems in applications. DSTA 2017. Springer proceedings in mathematics & statistics, vol 249. Springer, Cham, pp 385–399
31. Urbanowicz K, Firkowski M, Zarzycki Z (2016) Modelling water hammer in viscoelastic pipelines: short brief. J Phys Conf Ser 760:012–037
32. Urbanowicz K, Zarzycki Z (2015) Improved lumping friction model for liquid pipe flow. J Theor Appl Mech Pol 53(2):295–305
33. Wang X, Lin J, Keramat A, Ghidaoui MS, Meniconi S, Brunone B (2019) Matched-field processing for leak localization in a viscoelastic pipe: an experimental study. Mech Syst Signal Process 124:459–478
34. Zarzycki Z (1994) A hydraulic resistances of unsteady liquid flow in pipes. Szczecin University of Technology, Szczecin **(in Polish)**
35. Zarzycki Z, Urbanowicz K (2006) Modelling of transient flow during water hammer considering cavitation in pressure pipes. Chem Process Eng 27(3):915–933